Calcolo (2022) 59: 25
https://doi.org/10.1007/s10092-022-00468-3

High-order interpolatory Serendipity Virtual Element Method for semilinear parabolic problems

Sergio A. Gómez[1,2]

Received: 11 November 2021 / Revised: 27 April 2022 / Accepted: 2 May 2022 /
Published online: 14 June 2022

Abstract
We present an efficient method for the numerical approximation of a general class of two dimensional semilinear parabolic problems on polygonal meshes. The proposed approach takes advantage of the properties of the serendipity version of the Virtual Element Method, which not only reduces the number of degrees of freedom compared to the original Virtual Element Method, but also allows for the introduction of an approximation of the nonlinear term that is computable from the degrees of freedom of the discrete solution with a low computational cost, thus significantly improving the efficiency of the method. An error analysis for the semi-discrete formulation is carried out, and an optimal estimate for the error in the L_2-norm is obtained. The accuracy and efficiency of the proposed method when combined with a second order Strang operator splitting time discretization is illustrated in our numerical experiments, with approximations up to order 6.

Keywords Serendipity Virtual Element Method · Interpolant operator · Operator splitting method · Semilinear parabolic equations

Mathematics Subject Classification 65M60 · 65M12 · 65M15

1 Introduction

In this work we present an interpolatory or quasi-interpolatory Serendipity Virtual Element Method (S-VEM) applied to semilinear parabolic equations on a space–time domain $Q_T = \Omega \times (0, T)$, where $\Omega \subset \mathbb{R}^2$ is a polygonal domain and $T > 0$

✉ Sergio A. Gómez
sergio.gomez01@universitadipavia.it; gomezs@usi.ch

[1] Dipartimento di Matematica "F. Casorati", Università di Pavia, Via Ferrata 5, 27100 Pavia, Italy

[2] Faculty of Informatics, Università della Svizzera italiana, Via Buffi 13, 6900 Lugano, Switzerland

$$\frac{\partial u}{\partial t} - \Delta u + f(u) = 0, \quad \text{in } Q_T, \tag{1.1a}$$

$$\nabla u \cdot \boldsymbol{n} = 0, \quad \text{on } \partial\Omega \times (0, T], \tag{1.1b}$$

$$[r]u(\mathbf{x}, 0) = u_0(\mathbf{x}), \quad \text{in } \Omega. \tag{1.1c}$$

The nonlinear function $f : \mathbb{R} \to \mathbb{R}$ is assumed to be globally Lipschitz continuous, i.e., there exists a constant $L_f > 0$ such that the following bound holds

$$|f(x) - f(y)| \leq L_f |x - y| \quad \forall x, y \in \mathbb{R}. \tag{1.2}$$

The model (1.1a, 1.1b, 1.1c) is found in many important applications such as: battery modeling [33], crystals growth [23], population dynamics [29], and in many other models in chemistry [27, 34] and biology [25]. However, given the different nature of nonlinear terms, the task of finding exact solutions for such kind of problems becomes extremely demanding or even impossible. For that reason, there is a high interest in the development of efficient, accurate and robust numerical methods to approximate their solution. Since this work specifically concerns the advantages of the serendipity version of the Virtual Element Method applied to the problem (1.1a, 1.1b, 1.1c), an extensive list of numerical methods previously applied to this problem is out of our scope.

The Virtual Element Method (VEM) is a novel technique for the numerical approximation of PDEs, introduced by Beirão da Veiga *et al.* in [9] for an elliptic problem, and can be seen as a sensible extension of the classical finite element method to meshes with almost general polygonal elements. Discrete VEM spaces contain non-polynomial functions; however, such functions are not needed to be expressly known, as the discrete operators are computed through projections onto the space of piecewise polynomials of a given degree, which are computable using only some suitably chosen degrees of freedom (DoFs). Besides the advantages that come from the versatility of polygonal meshes, such as the natural use of "non-conforming" grids, more efficient and easier adaptivity and geometric approximation, robustness to mesh deformation, among others; the Virtual Element Method also allows for the imposition of conformity conditions on the global discrete spaces without struggling to explicitly compute their basis functions.

So far, the Virtual Element Method has been successfully applied to many important physical applications. In particular, recent efforts have been devoted to show the accuracy and advantages of this method in the numerical approximation of the solution to nonlinear problems such as: the Cahn–Hilliard equation [8, 24], models in cardiology [7], nonlinear elasticity [18], the nonlinear Brinkman equation [22, 28], bulk-surface reaction–diffusion systems [21], pattern formation [19]; and semilinear elliptic [5, 14], hyperbolic [2] and parabolic [1] equations.

In this work we aim to extend the idea of Adak and Natarajan in [3] to high-order approximations. In [3], the authors proposed a VEM discretization of the sine–Gordon equation with an interpolatory approximation of the nonlinear term, thus significantly reducing the computational cost of the method at each time

step. Nevertheless, the main limitation of the technique in [3] is that it is only valid for approximations with $k = 1$, i.e., with the same order of convergence as polynomial approximations of degree $k = 1$. This is due to the fact that for $k \geq 2$, the method requires some internal-moment DoFs, which unfortunately prevents a direct extension to high order approximations (see Remark 3.3 and Section 7 in [3] dedicated to discuss this limitation). Our idea to overcome this severe restriction relies on the serendipity version of the VEM, introduced by Beirão da Veiga *et al.* in [11], and later discussed by Russo in [30]. The main motivation of the S-VEM is indeed to reduce the number of internal-moment DoFs. Moreover, under certain conditions on the mesh, it is possible to completely eliminate them. It is also worth mentioning that the Serendipity VEM on quadrilaterals does not suffer from distortion as it is common for the serendipity FEM, see [11].

The main novelty and features of the proposed scheme are summarized as follows:

a) To the best of our knowledge, this is the first time to use the S-VEM as spatial discretization for semilinear parabolic problems; for which the enhanced VEM has been preferred.
b) An interpolant of the nonlinear term in the S-VEM space is introduced in the semi-discrete formulation. Under a certain condition on the degree of accuracy k that is associated with the geometric properties of the mesh, such interpolant is computed by simply evaluating the nonlinear term $f(\cdot)$ at the DoFs of the discrete solution. Thus, significantly reducing the computational cost of the method, as it completely avoids the use of numerical quadratures at each time step.
c) An optimal error estimate for the semi-discrete formulation in the L_2-norm is proven in spite of the use of such interpolant to approximate the nonlinear term.
d) When the time variable is discretized by the symmetric Strang - operator splitting (SS-OS) time marching scheme, the nonlinear substeps can be decomposed as a set of completely independent one dimensional nonlinear problems, which renders the method naturally suitable for parallel implementations.
e) In those elements of the mesh (if any) where the condition on the degree k is not satisfied, the interpolant of the nonlinear term is not computable from the DoFs of the discrete solution. In that case, we use a quasi-interpolatory approximation of the nonlinear term that also belongs to the local VEM space but is computable. Optimal error estimates and suitability for a parallel implementation are preserved.

The paper is structured as follows: in Sect. 2 we present the basic ideas and necessary projections for the description of the proposed method in the case when no internal-moment DoFs are needed, that throughout the paper we will refer to as "the ideal case". Optimal error estimates of order $\mathcal{O}(h^{k+1})$ in the L_2-norm are proven for the S-VEM semi-discrete formulation in Sect. 3. In Sect. 4, an efficient fully-discrete scheme, obtained by combining our interpolatory S-VEM discretization in space with a symmetric Strang - Operator Splitting time marching scheme is presented. The extension of the method to the general case when some

internal-moment DoFs are needed, as well as the most important differences in the error estimate and the fully-discrete scheme are discussed in Sect. 5. Some numerical experiments, validating the accuracy and efficiency of the proposed method are included in Sect. 6. We end this work with some concluding remarks in Sect. 7.

2 Serendipity VEM discretization

Let $\mathcal{T}_h$ be a polygonal partition of Ω and let $h := \max\left\{h_E \mid E \in \mathcal{T}_h\right\}$ be the mesh size, where h_E denotes the diameter of E. We first define, for each polygon $E \in \mathcal{T}_h$, the following enlarged local Virtual Element space [6]:

$$\widetilde{V}_k(E) := \left\{ v \in \mathcal{C}^0\left(\overline{E}\right) : \ v|_e \in \mathbb{P}_k(e) \ \forall \text{ edge } e, \ \Delta v \in \mathbb{P}_k(E) \right\},$$

where $\mathbb{P}_k(e)$ and $\mathbb{P}_k(E)$ denote the spaces of polynomials of degree at most $k \geq 1$ on e and E, respectively.

The DoFs uniquely identifying a function $v \in \widetilde{V}_k(E)$ are choosen as the following linear functionals

i) The values of v at the vertices of E.
ii) The values of v at the $(k-1)$ internal Gauss-Lobatto nodes on each edge e of E.
iii) The internal-moments: $\dfrac{1}{|E|}\displaystyle\int_E v m_\alpha^E d\boldsymbol{x}, \ \alpha = 1, \ldots, r_k$, where $\left\{m_\alpha\right\}_{\alpha=1}^{r_k}$ is a basis of $\mathbb{P}_k(E)$ and $r_k := \dim(\mathbb{P}_k(E))$.

The space $\widetilde{V}_k(E)$ requires many more internal DoFs than the original VEM space presented in [9], but it readily provides enough information to compute the L_2-projection of any $v \in \widetilde{V}_k(E)$ onto $\mathbb{P}_k(E)$. In practice, a subspace of $\widetilde{V}_k(E)$ still containing all polynomials of degree at most k on E, is used as local VEM space. The basic idea to construct such subspace is to take the set of functions in $\widetilde{V}_k(E)$ sharing some internal-moment DoFs with their projection onto the space $\mathbb{P}_k(E)$; which gives origin to the so called, *enhanced* [6] and *serendipity* [11] versions of the VEM.

We first focus on the ideal case, where the Serendipity VEM does not require any internal-moment DoFs. An integer number $\eta_E \geq 3$ is associated with each element $E \in \mathcal{T}_h$, where η_E is defined as the number of distinct straight lines containing at least one edge of E. In particular, if E is an N-sided strictly convex polygon without split edges, then $\eta_E = N$. In the ideal case, the degree of accuracy k satisfies the condition: $k < \min\left\{\eta_E \mid E \in \mathcal{T}_h\right\}$; which in the spirit of the Serendipity VEM, allows for the definition of a global discrete space whose associated DoFs are all node evaluations at the skeleton of the mesh, without requiring any internal-moment degree of freedom from the set iii).

The following projectors are needed to define the local S-VEM space and to present our semi-discrete formulation:

- The Ritz–Galerkin projection $\pi_{k,E}^{\nabla} : H^1(E) \to \mathbb{P}_k(E)$ defined as follows

$$\int_E \nabla\left(\pi^{\nabla}_{k,E}(v) - v\right) \cdot \nabla p_k d\boldsymbol{x} = 0 \quad \forall p_k \in \mathbb{P}_k(E),$$

$$\oint_{\partial E} \pi^{\nabla}_{k,E}(v) dS = \oint_{\partial E} v dS, \ (k=1), \quad \text{or} \quad \int_E \pi^{\nabla}_{k,E}(v) d\boldsymbol{x} = \int_E v d\boldsymbol{x}, \ (k>1).$$

Using the Green's formula, the projection $\pi^{\nabla}_{k,E}(\cdot)$ is computable for any $v \in \widetilde{V}_k(E)$ using the degrees of freedom i), ii) and iii), see [9, Sect. 4.5].

- The standard L_2-orthogonal projector $\pi^0_{k,E} : L_2(E) \to \mathbb{P}_k(E)$, defined by

$$\int_E \left(\pi^0_{k,E}(v) - v\right) p_k d\boldsymbol{x} = 0 \quad \forall p_k \in \mathbb{P}_k(E),$$

which is directly computable from the set of DoFs iii).

- The "boundary" projector $\pi^{\partial}_{k,E} : H^1(E) \to \mathbb{P}_k(E)$ such that

$$\oint_{\partial E} \left(\pi^{\partial}_{k,E}(v) - v\right) p_k \, dS = 0 \quad \forall p_k \in \mathbb{P}_k(E), \tag{2.1}$$

that is well-defined under the condition $k < \eta_E$, and can be computed using only the boundary DoFs in sets i) and ii).

In the ideal case, the local S-VEM space $V^S_k(E) \subset \widetilde{V}_k(E)$ is defined as

$$V^S_k(E) := \left\{ v \in \widetilde{V}_k(E) \, : \, \int_E \left(v - \pi^{\partial}_{k,E}(v)\right) m^E_\alpha d\boldsymbol{x} \ = \ 0, \ \alpha = 1, \dots, r_k \right\},$$

that only requires the boundary DoFs from sets i) and ii). Therefore, for an N-sided polygon E, $\dim\left(V^S_k(E)\right) = Nk$. The global S-VEM space is consequently defined as

$$V^S_k\left(\mathcal{T}_h\right) := \left\{ v_h \in \mathcal{C}^0\left(\overline{\Omega}\right) \, : \, v_h|_E \in V^S_k(E) \ \forall E \in \mathcal{T}_h \right\}.$$

A representation of the DoFs for the local space of the original VEM in [9], for different N-sided polygons and the maximum degree k satisfying the aforementioned condition is presented in Fig. 1. We emphasize that, in all these cases, the local space $V^S_k(E)$ does not require any of the internal-moment DoFs represented by red squares in the figure.

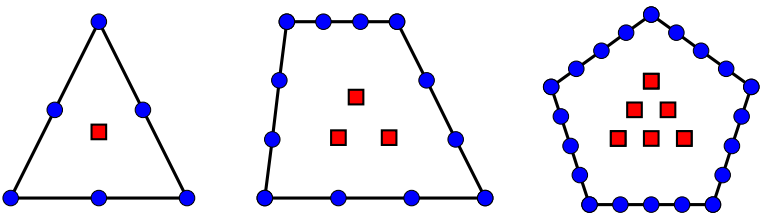

Fig. 1 Degrees of freedom for the original VEM space with degree $k = 2$ (triangles), $k = 3$ (quadrilaterals), and $k = 4$ (pentagons). Blue dots represent nodal evaluations, and red squares represent internal moments

As mentioned before, any function $v \in V_k^S(E)$ is uniquely determined by its boundary DoFs. Denoting by $d_{k,E}^S = \dim(V_k^S(E))$, and numbering the nodes associated with the DoFs as $\boldsymbol{\xi}_i$, with $i = 1, \dots, d_{k,E}^S$, we can define the linear functionals $\mathrm{dof}_i : V_k^S(E) \to \mathbb{R}$ as

$$\mathrm{dof}_i(v) := v(\boldsymbol{\xi}_i) \quad \forall v \in V_k^S(E). \tag{2.2}$$

A natural basis arise, by taking the canonical basis functions $\left\{\phi_i\right\}_{i=1}^{d_{k,E}^S}$ satisfying

$$\mathrm{dof}_i(\phi_j) = \delta_{ij}, \quad i,j = 1, \dots, d_{k,E}^S.$$

The following interpolatory representation is then obtained for each $v \in V_k^S(E)$

$$v(\boldsymbol{x}) = \sum_{i=1}^{d_{k,E}^S} \mathrm{dof}_i(v)\phi_i(\boldsymbol{x}) = \sum_{i=1}^{d_{k,E}^S} v(\boldsymbol{\xi}_i)\phi_i(\boldsymbol{x}); \tag{2.3}$$

such representation allows us to define the interpolant operator $\mathcal{I}_h^k : \mathcal{C}^0\left(\overline{\Omega}\right) \to V_k^S\left(\mathcal{T}_h\right)$ whose restriction to each element $E \in \mathcal{T}_h$ is defined as follows: for all $g \in \mathcal{C}^0\left(\overline{E}\right)$,

$$\mathcal{I}_h^{k,E} g(\boldsymbol{x}) := \sum_{i=1}^{d_{k,E}^S} \mathrm{dof}_i(g)\phi_i(\boldsymbol{x}) = \sum_{i=1}^{d_{k,E}^S} g(\boldsymbol{\xi}_i)\phi_i(\boldsymbol{x}). \tag{2.4}$$

2.1 Semi-discrete formulation

The weak formulation of the model problem (1.1a, 1.1b, 1.1c) is: find $u \in L_2\left(0, T, H^1(\Omega)\right)$ with $u_t \in L_2\left(0, T, H^{-1}(\Omega)\right)$ such that

$$m\left(\frac{\partial u}{\partial t}; v\right) + a(u; v) + m(f(u); v) = 0 \quad \forall v \in H^1(\Omega), \tag{2.5}$$

where $a(\cdot;\cdot) : H^1(\Omega) \times H^1(\Omega) \to \mathbb{R}$ and $m(\cdot;\cdot) : L_2(\Omega) \times L_2(\Omega) \to \mathbb{R}$ are the bilinear forms defined as

$$a(u; v) := \int_\Omega \nabla u \cdot \nabla v d\boldsymbol{x}, \quad m(u; v) := \int_\Omega uv d\boldsymbol{x}.$$

Analogously, our semi-discrete interpolatory S-VEM formulation seeks an approximation $u_h \in V_k^S\left(\mathcal{T}_h\right)$ such that for all test functions $v_h \in V_k^S\left(\mathcal{T}_h\right)$ it satisfies

$$m_h\left(\frac{\partial u_h}{\partial t}; v_h\right) + a_h\left(u_h; v_h\right) + m_h\left(\mathcal{I}_h^k f(u_h); v_h\right) = 0, \tag{2.6a}$$

$$u_h^0 = \mathcal{I}_h^k u_0, \tag{2.6b}$$

where the bilinear forms $a_h : V_k^S(\mathcal{T}_h) \times V_k^S(\mathcal{T}_h) \to \mathbb{R}$ and $m_h : V_k^S(\mathcal{T}_h) \times V_k^S(\mathcal{T}_h) \to \mathbb{R}$ are constructed as the sum of local contributions as

$$a_h(u_h; v_h) = \sum_{E \in \mathcal{T}_h} a_h^E(u_h; v_h), \qquad m_h(u_h; v_h) = \sum_{E \in \mathcal{T}_h} m_h^E(u_h; v_h).$$

For each element $E \in \mathcal{T}_h$, the restrictions $a_h^E(\cdot;\cdot)$ and $m_h^E(\cdot;\cdot)$ are split into a consistency and a stability parts by

$$a_h^E(u_h; v_h) := a^E\Big(\pi_{k,E}^{\nabla}(u_h); \pi_{k,E}^{\nabla}(v_h)\Big) + s_a^E\Big(\Big(I - \pi_{k,E}^{\nabla}\Big)u_h; \Big(I - \pi_{k,E}^{\nabla}\Big)v_h\Big), \tag{2.7a}$$

$$m_h^E(u_h; v_h) := m^E\Big(\pi_{k,E}^{0}(u_h); \pi_{k,E}^{0}(v_h)\Big) + s_m^E\Big(\Big(I - \pi_{k,E}^{0}\Big)u_h; \Big(I - \pi_{k,E}^{0}\Big)v_h\Big), \tag{2.7b}$$

where I denotes the identity operator and the stabilization terms $s_a^E(\cdot;\cdot)$, $s_m^E(\cdot;\cdot)$ are symmetric bilinear forms scaling as $a^E(\cdot;\cdot)$ and $m^E(\cdot;\cdot)$, respectively; more precisely, there exist mesh-independent positive constants $\alpha_1, \alpha_2, \beta_1, \beta_2$ such that

$$\begin{aligned} \alpha_1 a^E(v_h; v_h) \le s_a^E(v_h; v_h) \le \alpha_2 a^E(v_h; v_h) \quad \forall v_h \in V_k^S(E) \cap \mathrm{Ker}(\pi_k^{\nabla}), \\ \beta_1 m^E(v_h; v_h) \le s_m^E(v_h; v_h) \le \beta_2 m^E(v_h; v_h) \quad \forall v_h \in V_k^S(E) \cap \mathrm{Ker}(\pi_k^{0}). \end{aligned}$$

In fact, there are many possible choices for the stability terms; however, in our implementation we will limit ourselves to use a very simple stabilization proposed in [9], namely, the *dofi-dofi*. For a thorough study of different stability choices, see [12, 26]. By construction, both $a_h(\cdot;\cdot)$ and $m_h(\cdot;\cdot)$ satisfy the following two important conditions:

– **k-Polynomial consistency:** For every element $E \in \mathcal{T}_h$ we have

$$a_h^E(v_h; p_k) = a^E(v_h; p_k) \quad \forall v_h \in V_k^S(E),\ \forall p_k \in \mathbb{P}_k(E), \tag{2.8a}$$

$$m_h^E(v_h; p_k) = m^E(v_h; p_k) \quad \forall v_h \in V_k^S(E),\ \forall p_k \in \mathbb{P}_k(E). \tag{2.8b}$$

– **Stability:** There exist mesh-independent positive constants $\alpha_*,\ \alpha^*,\ \beta_*,\ \beta^*$ such that

$$\alpha_* a^E(v_h; v_h) \le a_h^E(v_h; v_h) \le \alpha^* a^E(v_h; v_h) \quad \forall v_h \in V_k^S(E), \tag{2.9a}$$

$$\beta_* m^E(v_h; v_h) \le m_h^E(v_h; v_h) \le \beta^* m^E(v_h; v_h) \quad \forall v_h \in V_k^S(E). \tag{2.9b}$$

The last term in the semi-discrete variational formulation (2.6a) satisfies the following crucial identity

$$
\begin{aligned}
m_h\left(\mathcal{I}_h^k f(u_h);\phi_i\right) &= \sum_{E\in\mathcal{T}_h} m_h^E\left(\mathcal{I}_h^{k,E} f(u_h);\phi_i\right) \\
&\overset{(2.3)}{=} \sum_{E\in\mathcal{T}_h}\sum_{j=1}^{d_{k,E}^S} \mathrm{dof}_j\left(f\left(u_h\right)\right) m_h^E\left(\phi_j;\phi_i\right) \\
&\overset{(2.4)}{=} \sum_{E\in\mathcal{T}_h}\sum_{j=1}^{d_{k,E}^S} f\left(u_h\left(\xi_j\right)\right) m_h^E\left(\phi_j;\phi_i\right) \\
&\overset{(2.3)}{=} \sum_{E\in\mathcal{T}_h}\sum_{j=1}^{d_{k,E}^S} f\left(\mathrm{dof}_j(u_h)\right) m_h^E\left(\phi_j;\phi_i\right),
\end{aligned}
\tag{2.10}
$$

which clearly shows that, in the ideal case, the computation of the nonlinear term requires only the matrix representation of the bilinear form $m_h(\cdot;\cdot)$ and the evaluation of $f(\cdot)$ at the DoFs of the discrete solution u_h.

Remark 1 Applying stabilization in the last term of (2.6a) in the semi-discrete formulation is not necessary to obtain optimal convergence, but it can be computationally convenient, as shown in Sect. 4.

Remark 2 The initial condition approximation $u_h^0 = \mathcal{I}_h^k u_0$ in (2.6b) is suitable for imposing random initial data, which is commonly of interest in this kind of problems.

3 Error analysis

This section is devoted to get an optimal error estimate in the L_2-norm for the solution to the semi-discrete formulation (2.6a, 2.6b). The main ideas are taken from the error analysis carried out in [35] for the enhanced VEM applied to linear parabolic problems and its recent extensions to semilinear parabolic problems [1, 4, 5]. Nonetheless, in Theorem 1 we address the following differences:

- The approximated solution is sought in the S-VEM space $V_k^S\left(\mathcal{T}_h\right)$.
- The nonlinear term is approximated by its interpolant $\mathcal{I}_h^k f(u_h) \in V_k^S\left(\mathcal{T}_h\right)$. The term $m_h\left(\mathcal{I}_h^k f(u_h);v_h\right)$ in the semi-discrete formulation (2.6a) includes also a stabilization part, that was not present in the formulation in [3] for the sine-Gordon equation. This choice is computationally convenient when using an operator splitting time marching scheme, while retaining the same optimal convergence.
- Pure homogeneous Neumann boundary conditions are considered.

In what follows we will make the following assumptions on the mesh:

Assumption 1 There exists a constant $\rho > 0$, such that every element $E \in \mathcal{T}_h$ is star-shaped with respect to a ball $B := B_{\rho h_E}(z)$ centered at $z \in E$ and with radius ρh_E, where $h_E := \text{diam}(E)$. In addition, every edge e of E satisfies $|e| \geq \rho h_E$.

The above assumption guarantees that the following condition holds: *for each $E \in \mathcal{T}_h$, there exists a "virtual triangulation" $\widetilde{\mathcal{T}}_E$ of E such that $\widetilde{\mathcal{T}}_E$ is uniformly shape regular and quasi-uniform. The corresponding mesh size of the auxiliary triangulation $\widetilde{\mathcal{T}}_E$ is proportional to h_E and each edge of E is a side of a triangle in $\widetilde{\mathcal{T}}_E$.*

The elliptic projection operator $\mathcal{P}_h : H^1(\Omega) \to V_k^S(\mathcal{T}_h)$, is defined for each function $u \in H^1(\Omega)$ as the only element $\mathcal{P}_h(u) \in V_k^S(\mathcal{T}_h)$ satisfying

$$\begin{cases} a_h\big(\mathcal{P}_h(u); v_h\big) = a\big(u; v_h\big) \quad \forall v_h \in V_k^S(\mathcal{T}_h), \\ \displaystyle\int_\Omega \mathcal{P}_h(u) d\boldsymbol{x} = 0. \end{cases} \tag{3.1}$$

Since $\mathcal{P}_h(u)$ is the solution to the variational problem (3.1), by the coercivity and continuity of $a_h(\cdot;\cdot)$ and the continuity of the linear functional $a(u;\cdot)$, the projection operator $\mathcal{P}_h$ is well-defined. Furthermore, we can prove the following estimate as in [35, Lemma 3.1].

Lemma 1 *Let Ω be a convex domain, and $u \in H^{k+1}(\Omega)$. Under Assumption 1, there exists a constant $C_\alpha > 0$, depending on α_* and α^* in (2.9a) but independent of h such that*

$$\big\|\mathcal{P}_h(u) - u\big\|_{L_2(\Omega)} \leq C_\alpha h^{k+1} |u|_{H^{k+1}(\Omega)}. \tag{3.2}$$

Using standard arguments as in [9] and the classical Dupont-Scott theory in [13], the following estimates for the interpolant $\mathcal{I}_h^k(\cdot)$ and the projection $\pi_k^0(\cdot)$ are obtained.

Lemma 2 *Under Assumption 1, if $u \in H^{k+1}(\Omega)$, there exists a positive constant C_I, depending only on k and ρ, such that the interpolant $\mathcal{I}_h^k u \in V_k^S(\mathcal{T}_h)$ satisfies*

$$\Big\|u - \mathcal{I}_h^k u\Big\|_{L_2(E)} + h_E \Big|u - \mathcal{I}_h^k u\Big|_{H^1(E)} \leq C_I h_E^{k+1} |u|_{H^{k+1}(E)} \quad \forall E \in \mathcal{T}_h. \tag{3.3}$$

Lemma 3 *Under Assumption 1, for each element $E \in \mathcal{T}_h$, if $u \in H^{k+1}(E)$, there exists a polynomial $u_\pi \in \mathbb{P}_k(E)$, and a positive constant C_π, depending only on k and ρ, such that*

$$\big\|u - u_\pi\big\|_{L_2(E)} + h_E |u - u_\pi|_{H^1(E)} \leq C_\pi h_E^{k+1} |u|_{H^{k+1}(E)}. \tag{3.4}$$

In Lemma 4, a norm equivalence for the S-VEM space is introduced in order to exploit the Lipschitz property of $f(\cdot)$ in the analysis.

Lemma 4 *Under Assumption 1, there exist two positive constants c_1 and c_2 depending on the shape regularity and quasi-uniformity parameters of the auxiliary triangulation $\widetilde{\mathcal{T}}_E$ of E such that*

$$c_1 h_E \|\chi(v)\|_{l_2} \leq \|v\|_{L_2(E)} \leq c_2 h_E \|\chi(v)\|_{l_2}, \tag{3.5}$$

where $\chi : V_k^S(E) \to \mathbb{R}^{d_{k,E}^S}$ *is defined by* $\chi(v) := \left(\mathrm{dof}_i v\right)_{i=1}^{d_{k,E}^S}$.

Lemma 4 is an extension of the classical results in [20] for finite element spaces and can be proven following the arguments used by Chen and Huang in [17, Thm. 4.5 and Corollary 4.6].

From the above Lemma we can derive the following important bound in our error analysis.

Lemma 5 *The following bound holds for any* $u \in C^0\left(\overline{E}\right)$ *and* $u_h \in V_k^S(E)$

$$\left\|\mathcal{I}_h^k f(u) - \mathcal{I}_h^k f(u_h)\right\|_{L_2(E)} \leq \frac{c_2 L_f}{c_1}\left(\left\|\mathcal{I}_h^k u - u\right\|_{L_2(E)} + \|e_u\|_{L_2(E)}\right), \tag{3.6}$$

where $e_u := u - u_h$.

Proof By Lemma 4, and the Lipschitz continuity of $f(\cdot)$ we have

$$\begin{aligned}
\left\|\mathcal{I}_h^k f(u) - \mathcal{I}_h^k f(u_h)\right\|_{L_2(E)} &\overset{(3.5)}{\leq} c_2 h_E \left\|\chi\left(\mathcal{I}_h^k f(u) - \mathcal{I}_h^k f(u_h)\right)\right\|_{l_2} \\
&\overset{(2.2)}{=} c_2 h_E \left(\sum_{i=1}^{d_{k,E}^S} \left|f(u(\xi_i)) - f(u_h(\xi_i))\right|^2\right)^{\frac{1}{2}} \\
&\overset{(1.2)}{\leq} c_2 h_E L_f \left(\sum_{i=1}^{d_{k,E}^S} \left|u(\xi_i) - u_h(\xi_i)\right|^2\right)^{\frac{1}{2}} \\
&\overset{(2.2)}{=} c_2 h_E L_f \left\|\chi\left(\mathcal{I}_h^k u - u_h\right)\right\|_{L_2(E)} \\
&\overset{(3.5)}{\leq} \frac{c_2 L_f}{c_1} \left\|\mathcal{I}_h^k u - u_h\right\|_{L_2(E)},
\end{aligned}$$

To conclude the proof it suffices to use the triangle inequality in the last term. □

The following theorem provides the optimal error estimate for the semi-discrete formulation (2.6a, 2.6b) under suitable regularity conditions for the exact solution. We will use C to denote a generic constant independent of the mesh size h and the arguments of the functions in the proof will be omitted unless they are necessary.

Theorem 1 *Under Assumption 1. Let Ω be a convex domain, and u and u_h be the solutions to the variational problems (2.5) and (2.6a, 2.6b), respectively. For u and $f(u)$ smooth enough, there exists a positive constant C independent of h, such that for all $t \in (0,T]$ the following bound holds*

$$\begin{aligned}\left\|u_h(\cdot,t)-u(\cdot,t)\right\|_{L_2(\Omega)} \leq Ch^{k+1}\Big(&\left|u_0\right|_{H^{k+1}(\Omega)} + \left\|u_t\right\|_{L_1\left(0,t,H^{k+1}(\Omega)\right)}\\ &+\left\|u_t\right\|_{L_2\left(0,t,H^{k+1}(\Omega)\right)} + \left\|u\right\|_{L_2\left(0,t,H^{k+1}(\Omega)\right)}\\ &+\left\|f(u)\right\|_{L_2\left(0,t,H^{k+1}(\Omega)\right)}\Big).\end{aligned} \tag{3.7}$$

Proof We start decomposing $e_u := u - u_h$ as $e_u = \xi_u - \theta_h$, where $\xi_u = u - \mathcal{P}_h(u)$ and $\theta_h = u_h - \mathcal{P}_h(u)$. From Lemma 1 and the identity $u(\cdot,t) = u(\cdot,0) + \int_0^t u_t(\cdot,\tau)d\tau$ we have the following bound for ξ_u

$$\left\|\xi_u(\cdot,t)\right\|_{L_2(\Omega)} \leq Ch^{k+1}\Big(\left|u_0\right|_{H^{k+1}(\Omega)} + \left|u_t\right|_{L_1(0,t,H^{k+1}(\Omega))}\Big). \tag{3.8}$$

Therefore, in order to get the desired estimate, it only remains to bound $\left\|\theta_h(\cdot,t)\right\|_{L_2(\Omega)}$. We now proceed similarly as in [1]. Since $\theta_h \in V_k^S\left(\mathcal{T}_h\right)$, adding and subtracting appropriate terms in the semi-discrete formulation (2.6a), for any $v_h \in V_k^S\left(\mathcal{T}_h\right)$ we get

$$\begin{aligned}
&m_h\Big(\tfrac{\partial\theta_h}{\partial t};v_h\Big) + a_h\big(\theta_h;v_h\big)\\
&\quad= -m_h\big(I_h^k f(u_h);v_h\big) - m_h\Big(\tfrac{\partial}{\partial t}P_h(u);v_h\Big) - a_h\big(P_h(u);v_h\big)\\
&\quad\overset{(3.1)}{=} -m_h\big(I_h^k f(u_h);v_h\big) - m_h\Big(\tfrac{\partial}{\partial t}P_h(u);v_h\Big) - a\big(u;v_h\big)\\
&\quad\overset{(2.5)}{=} m\big(f(u);v_h\big) - m_h\big(I_h^k f(u_h);v_h\big) + m\Big(\tfrac{\partial u}{\partial t};v_h\Big) - m_h\Big(\tfrac{\partial}{\partial t}P_h(u);v_h\Big)\\
&\quad\overset{(2.7b)}{=} \sum_{E\in T_h}\Bigg[\underbrace{m^E\big(f(u);v_h\big) - m_h^E\big(I_h^k f(u_h);v_h\big)}_{T_1^E} + \underbrace{m^E\Big(\tfrac{\partial u}{\partial t};v_h\Big) - m_h^E\Big(\tfrac{\partial}{\partial t}P_h(u);v_h\Big)}_{T_2^E}\Bigg],
\end{aligned} \tag{3.9}$$

hence, we will look for local estimates of T_1^E and T_2^E on each element $E \in \mathcal{T}_h$.

By the k-polynomial consistency property (2.8b), we can decompose T_1^E as

$$\begin{aligned}
T_1^E &\overset{(2.8b)}{=} m^E\big(f(u) - \pi_k^0(f(u));v_h\big) + m^E\big(\pi_k^0(f(u)) - \pi_k^0\big(I_h^k(f(u))\big);v_h\big)\\
&\quad + m_h^E\big(\pi_k^0\big(I_h^k f(u)\big) - I_h^k f(u_h);v_h\big)\\
&= R_1 + R_2 + R_3.
\end{aligned} \tag{3.10}$$

By the Cauchy-Schwarz inequality and Lemma 3, it is easy to see that

$$|R_1| \overset{(3.4)}{\leq} C_\pi h^{k+1} |f(u)|_{H^{k+1}(E)} \|v_h\|_{L_2(E)}. \tag{3.11}$$

On the other hand, by the stability of the L_2-orthogonal projection $\pi_k^0(\cdot)$ and Lemma 2 we have

$$|R_2| \leq \left\| f(u) - \mathcal{I}_h^k f(u) \right\|_{L_2(E)} \|v_h\|_{L_2(E)} \overset{(3.3)}{\leq} C_I h^{k+1} |f(u)|_{H^{k+1}(E)} \|v_h\|_{L_2(E)}. \tag{3.12}$$

To bound R_3, we first observe that by the triangle inequality, the stability of the L_2 -orthogonal projection and Lemmas 2 and 3 we have

$$\begin{aligned} \left\| \pi_k^0\left(\mathcal{I}_h^k f(u)\right) - \mathcal{I}_h^k f(u) \right\|_{L_2(E)} &\leq \left\| \pi_k^0\left(\mathcal{I}_h^k f(u)\right) - \pi_k^0(f(u)) \right\|_{L_2(E)} \\ &\quad + \left\| \pi_k^0(f(u)) - f(u) \right\|_{L_2(E)} \\ &\quad + \left\| f(u) - \mathcal{I}_h^k f(u) \right\|_{L_2(E)} \\ &\leq \left(2C_I + C_\pi\right) h^{k+1} |f(u)|_{H^{k+1}(E)}. \end{aligned} \tag{3.13}$$

Lemma 5 and the bound (3.13), together with the triangle inequality and the continuity of $m_h(\cdot;\cdot)$ provide the following estimate for R_3:

$$\begin{aligned} |R_3| &\overset{(2.9b)}{\leq} \beta^* \left\| \pi_k^0\left(\mathcal{I}_h^k f(u)\right) - \mathcal{I}_h^k f(u_h) \right\|_{L_2(E)} \|v_h\|_{L_2(E)} \\ &\leq \beta^* \left(\left\| \pi_k^0\left(\mathcal{I}_h^k f(u)\right) - \mathcal{I}_h^k f(u) \right\|_{L_2(E)} + \left\| \mathcal{I}_h^k f(u) - \mathcal{I}_h^k f(u_h) \right\|_{L_2(E)} \right) \|v_h\|_{L_2(E)} \\ &\overset{(3.6)}{\leq} C \left(\left\| \pi_k^0\left(\mathcal{I}_h^k f(u)\right) - \mathcal{I}_h^k f(u) \right\|_{L_2(E)} + \left\| \mathcal{I}_h^k u - u \right\|_{L_2(E)} + \|e_u\|_{L_2(E)} \right) \|v_h\|_{L_2(E)} \\ &\overset{(3.13)}{\leq} C \left(h^{k+1} |f(u)|_{H^{k+1}(E)} + h^{k+1} |u|_{H^{k+1}(E)} + \|e_u\|_{L_2(E)} \right) \|v_h\|_{L_2(E)}. \end{aligned} \tag{3.14}$$

In a similar way, decomposing

$$\begin{aligned} &m^E\left(u_t; v_h\right) - m_h^E\left(\mathcal{P}_h\left(u_t\right); v_h\right) \\ &\qquad = m^E\left(u_t - \pi_k^0\left(u_t\right); v_h\right) - m_h^E\left(\mathcal{P}_h\left(u_t\right) - \pi_k^0\left(u_t\right); v_h\right), \end{aligned}$$

and applying similar steps as before, by the commutativity of $\frac{\partial}{\partial t}(\cdot)$ and $\mathcal{P}_h(\cdot)$, we get the following bound for T_2^E

$$\left| T_2^E \right| \leq C h^{k+1} \left| u_t \right|_{H^{k+1}(E)}. \tag{3.15}$$

Integrating from 0 to t at both sides of (3.9) and taking $v_h = \theta_h$; since $a_h\left(\theta_h; \theta_h\right) \geq 0$, by the estimate (3.8) for ξ_u, the bounds (3.11)–(3.15) and Young's inequality, we get the following estimate

$$
\begin{aligned}
\left\|\theta_h(\cdot,t)\right\|^2_{L_2(\Omega)} &\overset{(2.9b)}{\leq} \beta_*^{-1} m_h\big(\theta_h(\cdot,t);\theta_h(\cdot,t)\big) + 2\beta_*^{-1}\int_0^t a_h\big(\theta_h;\theta_h\big)d\tau \\
&\leq Cm_h\big(\theta_h(\cdot,0);\theta_h(\cdot,0)\big) + C\int_0^t \left\|e_u\right\|_{L_2(\Omega)}\left\|\theta_h\right\|_{L_2(\Omega)}d\tau \\
&\quad + Ch^{k+1}\int_0^t \Big(|f(u)|_{H^{k+1}(\Omega)} + |u|_{H^{k+1}(\Omega)} + |u_t|_{H^{k+1}(\Omega)}\Big)\left\|\theta_h\right\|_{L_2(\Omega)}d\tau \\
&\leq Cm_h\big(\theta_h(\cdot,0);\theta_h(\cdot,0)\big) + C\int_0^t \Big(\left\|\xi_u\right\|_{L_2(\Omega)}\left\|\theta_h\right\|_{L_2(\Omega)} + \left\|\theta_h\right\|^2_{L_2(\Omega)}\Big)d\tau \\
&\quad + Ch^{k+1}\int_0^t \Big(|f(u)|_{H^{k+1}(\Omega)} + |u|_{H^{k+1}(\Omega)} + |u_t|_{H^{k+1}(\Omega)}\Big)\left\|\theta_h\right\|_{L_2(\Omega)}d\tau \\
&\overset{(3.8)}{\leq} Cm_h\big(\theta_h(\cdot,0);\theta_h(\cdot,0)\big) + \int_0^t C\left\|\theta_h(\cdot,\tau)\right\|^2_{L_2(\Omega)}d\tau \\
&\quad + Ch^{k+1}\Big(|u_0|^2_{H^{k+1}(\Omega)}\left\|u_t\right\|^2_{L_1(0,t,H^{k+1}(\Omega))} + \left\|u_t\right\|^2_{L_2(0,t,H^{k+1}(\Omega))} \\
&\quad + \left\|u\right\|^2_{L_2(0,t,H^{k+1}(\Omega))} + \left\|f(u)\right\|^2_{L_2(0,t,H^{k+1}(\Omega))}\Big),
\end{aligned}
$$

and by Grönwall's lemma, since $\theta_h(\cdot,0) = \Big(\mathcal{P}_h\big(u_0\big) - u_0\Big) + \Big(u_0 - \mathcal{I}_h^k u_0\Big)$, combined with the bound (3.8) for ξ_u, and the estimates (3.2)–(3.3), we get the desired estimate (3.7) in our theorem. □

Remark 3 The term $\left\|\pi_k^0\big(\mathcal{I}_h^k f(u)\big) - \mathcal{I}_h^k f(u)\right\|_{L_2(E)}$ in (3.13) must be treated with care, since a direct application of the bound in Lemma 3 leads to the appearance of the undesired term $\left|\mathcal{I}_h^k f(u)\right|_{H^{k+1}(E)}$, that would become an issue in the error analysis, since the stability of the interpolation operator $\mathcal{I}_h^k(\cdot)$ on the seminorm $|\cdot|_{H^{k+1}(E)}$ is not guaranteed. On the other hand, bound (3.13) is not necessary when the stability part of the last term of (2.6a) in the semi-discrete formulation is not considered.

4 Fully-discrete scheme

It is evident that the efficiency of any ODE solver applied to (2.6a, 2.6b) will be greatly benefited from the fast evaluation of the nonlinear term in our semi-discrete formulation. In this paper, we choose the second order symmetric Strang operator splitting (SS-OS) method [32] as time marching scheme to illustrate the advantages of the proposed technique.

Denoting by $\mathbf{M}$ and $\mathbf{A}$ the matrix representation of the bilinear forms $m_h(\cdot;\cdot)$ and $a_h(\cdot;\cdot)$, respectively; by the identity (2.10), the semi-discrete formulation (2.6a, 2.6b) can be written as a system of nonlinear differential equations as

$$
\mathbf{M}\frac{\mathrm{d}\boldsymbol{U}_h}{\mathrm{d}t} + \mathbf{A}\boldsymbol{U}_h + \mathbf{M}\boldsymbol{f}_h\big(\boldsymbol{U}_h\big) = \mathbf{0}, \tag{4.1}
$$

where $\boldsymbol{U}_h$ is the vector of the representation coefficients of u_h in the basis of $V_k^S\big(\mathcal{T}_h\big)$; and the components of the vector $\boldsymbol{f}_h(\boldsymbol{U}_h)$ are given by $\big(\boldsymbol{f}_h\big(\boldsymbol{U}_h\big)\big)_i = \mathrm{dof}_i\big(f(u_h)\big)$.

In the ideal case, $\boldsymbol{f}_h(\boldsymbol{U}_h)$ is the vector obtained from a component-wise evaluation of the nonlinear function $f(\cdot)$ at the entries of $\boldsymbol{U}_h$.

The SS-OS time marching scheme decomposes the system of differential equations (4.1) as a series of linear and nonlinear substeps, usually associated with diffusion and reaction terms, of the form

$\mathcal{DRD}$ decomposition:

$$\boldsymbol{U}_h^{(1)} = \mathcal{D}_{\tau/2}\big(\boldsymbol{U}_h^n\big), \quad \boldsymbol{U}_h^{(2)} = \mathcal{R}_{\tau}\Big(\boldsymbol{U}_h^{(1)}\Big), \quad \boldsymbol{U}_h^{n+1} = \mathcal{D}_{\tau/2}\Big(\boldsymbol{U}_h^{(2)}\Big), \tag{4.2a}$$

$\mathcal{RDR}$ decomposition:

$$\boldsymbol{U}_h^{(1)} = \mathcal{R}_{\tau/2}\big(\boldsymbol{U}_h^n\big), \quad \boldsymbol{U}_h^{(2)} = \mathcal{D}_{\tau}\Big(\boldsymbol{U}_h^{(1)}\Big), \quad \boldsymbol{U}_h^{n+1} = \mathcal{R}_{\tau/2}\Big(\boldsymbol{U}_h^{(2)}\Big), \tag{4.2b}$$

where $\tau = t_{n+1} - t_n$ and $\boldsymbol{U}_h^n$ is the vector approximation of $u_h(\cdot, t_n)$.

The efficiency of combining some discontinuous Galerkin methods with an interpolatory approximation of the nonlinear term as spatial discretization on classical meshes with the SS-OS time marching scheme was assessed by Castillo and Gómez in [15, 16].

A necessary condition to retain the second order accuracy of the full SS-OS step is that each substep in (4.2a, 4.2b) must be solved with a second order ODE solver itself. Although we are free to choose the solver for each step, implicit methods might be more appropriate. Conversely, if an explicit method were used, we would face a very restrictive CFL condition associated with the linear substeps, while for the nonlinear substeps the method might become unstable in the case of stiff nonlinearities.

From the discussion above we decide to apply the Crank-Nicolson method to each substep in (4.2a, 4.2b). For the $\mathcal{DRD}$ decomposition (4.2a) the resulting fully-discrete method reads

$$\Big(\mathbf{M} + \frac{\tau}{4}\mathbf{A}\Big)\boldsymbol{U}_h^{(1)} = \Big(\mathbf{M} - \frac{\tau}{4}\mathbf{A}\Big)\boldsymbol{U}_h^n, \tag{4.3a}$$

$$\boldsymbol{U}_h^{(2)} = \boldsymbol{U}_h^{(1)} - \frac{\tau}{2}\Big(\boldsymbol{f}_h\Big(\boldsymbol{U}_h^{(1)}\Big) + \boldsymbol{f}_h\Big(\boldsymbol{U}_h^{(2)}\Big)\Big), \tag{4.3b}$$

$$\Big(\mathbf{M} + \frac{\tau}{4}\mathbf{A}\Big)\boldsymbol{U}_h^{n+1} = \Big(\mathbf{M} - \frac{\tau}{4}\mathbf{A}\Big)\boldsymbol{U}_h^{(2)}. \tag{4.3c}$$

The following remarks are in order:

- The linear substeps (4.3a) and (4.3c) only consist in solving two linear systems with the same matrix. For a fixed time step τ such matrix is even the same at any time, which is advantageous since a preconditioner or a full Cholesky factorization can be computed just once at the beginning of the simulation.
- The nonlinear substep requires the solution of the nonlinear system (4.3b), which is completely independent for each component of the vector $\boldsymbol{U}_h^{(2)}$, and as such,

highly parallelizable. Note that we have cancelled matrix $\mathbf{M}$ at both sides of this equation. Such cancellation is only possible because stabilization was also applied to the nonlinear term in (2.6a); otherwise, a large coupled system of nonlinear equations would be obtained. If we apply the Newton's method to (4.3b) each linear iteration s reads

$$\left(\mathbf{I} + \frac{\tau}{2}\mathbf{D}_f\left(\boldsymbol{U}_h^{(2,s)}\right)\right)\boldsymbol{\delta}^{(s)} = \mathbf{b}_s, \tag{4.4a}$$

$$\boldsymbol{U}_h^{(2,s+1)} = \boldsymbol{U}_h^{(2,s)} - \boldsymbol{\delta}^{(s)}, \tag{4.4b}$$

where $\mathbf{I}$ is the identity matrix, $\mathbf{b}_s = \boldsymbol{U}_h^{(2,s)} - \boldsymbol{U}_h^{(1)} + \frac{\tau}{2}\left(\boldsymbol{f}_h\left(\boldsymbol{U}_h^{(2,s)}\right) + \boldsymbol{f}_h\left(\boldsymbol{U}_h^{(1)}\right)\right)$ and $\mathbf{D}_f(\boldsymbol{U}_h)$ is the diagonal matrix $\mathbf{D}_f\left(\boldsymbol{U}_h\right) = \mathrm{diag}\left(f'\left(\boldsymbol{U}_h\right)\right)$. Since matrix $\left(\mathbf{I} + \frac{\tau}{2}\mathbf{D}_f\left(\boldsymbol{U}_h^{(2,s)}\right)\right)$ is also diagonal, the solution of (4.4a) reduces to a trivial entry-by-entry division.

We end this section with the following well-posedness result of the fully-discrete scheme.

Proposition 1 *The fully-discrete schemes $\mathcal{DRD}$ and $\mathcal{RDR}$ are well-posed for any $0 < \tau < 2/L_f$.*

Proof Without loss of generality we will prove the well-posedness only for the $\mathcal{DRD}$ scheme.

Since matrix $\left(\mathbf{M} + \frac{\tau}{4}\mathbf{A}\right)$ is symmetric and positive definite, the existence of the solution of each linear substep in (4.3a) and (4.3c) is guaranteed.

On the other hand, each independent one dimensional problem in the nonlinear substeps (4.3b) is equivalent to find a fixed point of the function $g(x) = a - \frac{\tau}{2}f(x)$ for some constant a, which can be easily shown to be a contraction as long as $0 < \tau < 2/L_f$; therefore, under such condition, the existence of a unique solution to the nonlinear substeps is also guaranteed.

Existence and uniqueness of the full step in (4.3a, 4.3b, 4.3c) then proceed from those of each susbtep. □

5 Extension to arbitrary *k*

We now present an extension of the interpolatory S-VEM to the general case, when some internal-moment DoFs are needed. The main drawback in such case is that for $k \geq \eta_E$, condition (2.1) is not enough to define a projection due to the existence of $\mathbb{P}_k(E)$-bubbles. Hence, some additional internal-moment DoFs and a computable projection operator are needed.

Since for non-convex polygons the choice of the additional DoFs is more involved, see [11, Sect. 3], we will focus on the case of convex polygons. For convex

polygons, if the internal-moment DoFs up to order $k-\eta_E$ are added, the projection $\pi^S_{k,E} : \widetilde{V}_k(E) \to \mathbb{P}_k(E)$ defined in [30] for each $v_h \in \widetilde{V}_k(E)$ as

$$\left(\chi\left(\pi^S_{k,E}(v_h)\right), \chi\left(m^E_\alpha\right)\right)_{l_2} = \left(\chi(v_h), \chi\left(m^E_\alpha\right)\right)_{l_2}, \quad \alpha = 1, \dots, r_k,$$

is well-defined and computable from the DoFs of v_h by definition.

For any convex polygon $E \in \mathcal{T}_h$, if $k \geq \eta_E$, the local Serendipity VEM space is then defined as

$$V^S_k(E) := \left\{ v \in C^0\left(\overline{E}\right) : \int_E \left(v - \pi^S_{k,E}(v)\right) m^E_\alpha d\boldsymbol{x} = 0,\ r_{k-\eta_E} < \alpha \leq r_k \right\}.$$

and $d^S_{k,E} = kN_E + \dim(\mathbb{P}_{k-\eta_E}(E))$.

Unfortunately, the presence of these internal-moment DoFs prevents the direct extension of the variational formulation (2.6a, 2.6b) to the case when k does not satisfy the condition of the ideal case. This is due to the fact that the entries of the vector $\boldsymbol{f}_h(\boldsymbol{U}_h)$ in (4.1) corresponding to such DoFs consist of integrals of the form

$$\frac{1}{|E|}\int_E f(u_h) m_\alpha d\boldsymbol{x},\ \alpha = 1, \dots, r_{k-\eta_E},$$

that are not computable via the DoFs of u_h. To overcome this problem, we replace the interpolant $\mathcal{I}^k_h f(u_h)$ in the semi-discrete variational formulation (2.6a, 2.6b) by a computable quasi-interpolatory approximation in the space $V^S_k\left(\mathcal{T}_h\right)$ that will be denoted by $\widetilde{f}_h(u_h)$.

For clarity, we assume that the DoFs associated with $V^S_k(E)$ are arranged so that the first (kN_E) of them correspond to the boundary DoFs. Since every function in the space $V^S_k\left(\mathcal{T}_h\right)$ is uniquely determined by its DoFs, we set the DoFs of the quasi-interpolant $\widetilde{f}_h(u_h)$ on each element $E \in \mathcal{T}_h$ as

$$\begin{aligned} \mathrm{dof}_i\left(\widetilde{f}_h(u_h)\right) &:= \mathrm{dof}_i\left(f(u_h)\right) = f\left(u_h(\boldsymbol{\xi}_i)\right), \quad \text{for } i = 1, \dots, kN_E, \\ \mathrm{dof}_i\left(\widetilde{f}_h(u_h)\right) &:= \mathrm{dof}_i\left(f\left(\pi^0_{k,E}(u_h)\right)\right) = \frac{1}{|E|}\int_E f\left(\pi^0_{k,E}(u_h)\right) m^E_{\alpha(i)} d\boldsymbol{x}, \end{aligned} \tag{5.1a}$$

$$\text{for } i = kN_E + 1, \dots, d^S_{k,E}, \tag{5.1b}$$

with $\alpha(i) := i - kN_E$. Unlike the interpolant $\mathcal{I}^k_h f(u_h)$, the new approximation $\widetilde{f}_h(u_h) \in V^S_k(E)$ is computable via the DoFs of u_h as desired.

5.1 Extension of the error estimate

Most steps in the proof of the error estimate in Theorem 1 are still valid for this extension of the method. The main difference lies on the decomposition of the left-hand side of (3.10) after substituting $\mathcal{I}^k_h f(u_h)$ by $\widetilde{f}_h(u_h)$, where an additional term

$R_4 := m_h^E\left(\mathcal{I}_h^k f(u_h) - \widetilde{f}_h(u_h); v_h\right)$ arises. Such term can be bounded using the continuity of the bilinear form $m_h^E(\cdot;\cdot)$ and the following Lemma.

Lemma 6 *Let $\left\{m_\alpha^E\right\}_{\alpha=1}^{r_{k-\eta_E}}$ be a basis of $\mathbb{P}_{k-\eta_E}(E)$ that is uniformly bounded in the L_∞-norm as $\left\|m_\alpha^E\right\|_{L_\infty(E)} \leq 1,\ \alpha = 1,\dots,r_{k-\eta_E}$. For any $u_h \in V_k^S(E)$, the following bound holds*

$$\left\|\mathcal{I}_h^k f(u_h) - \widetilde{f}_h(u_h)\right\|_{L_2(E)} \leq \frac{c_2 L_f r_{k-\eta_E}}{c_1}\left(2\left\|e_u\right\|_{L_2(E)} + \left\|u - \pi_k^0(u)\right\|_{L_2(E)}\right).$$

Proof Using Lemma 4, the definition of $\widetilde{f}_h(u_h)$, and the Cauchy-Schwarz inequality we have

$$\begin{aligned}
\|\mathcal{I}_h^k f(u_h) - \widetilde{f}_h(u_h)\|_{L_2(E)} &\overset{(3.5)}{\leq} c_2 h_E \left\|\chi\left(\mathcal{I}_h^k f(u_h) - \widetilde{f}_h(u_h)\right)\right\|_{l_2} \\
&\overset{(5.1)}{=} \frac{c_2 h_E}{|E|}\left[\sum_{\alpha=1}^{r_{k-\eta_E}}\left(\int_E \left(f\left(u_h\right) - f\left(\pi_k^0\left(u_h\right)\right)\right) m_\alpha^E d\boldsymbol{x}\right)^2\right]^{\frac{1}{2}} \\
&\overset{(1.2)}{\leq} c_2 h_E L_f \left\|u_h - \pi_k^0\left(u_h\right)\right\|_{L_2(E)}\left[\sum_{\alpha=1}^{r_{k-\eta_E}} \frac{\left\|m_\alpha^E\right\|_{L_2(E)}^2}{|E|^2}\right]^{\frac{1}{2}} \\
&\leq \frac{c_2 L_f r_{k-\eta_E}}{c_1}\left\|u_h - \pi_k^0\left(u_h\right)\right\|_{L_2(E)}.
\end{aligned}$$

The assertion follows by the triangle inequality and the stability of the $\pi_k^0(\cdot)$ projection. □

An example of a polynomial basis satisfying the uniformly boundedness condition in the statement of the previous lemma is the scaled monomial basis defined in [9].

5.2 Implementation of the fully-discrete scheme

The matrix representation of the semi-discrete variational formulation becomes

$$\mathbf{M}\frac{\mathrm{d}\boldsymbol{U}_h}{\mathrm{d}t} + \mathbf{A}\boldsymbol{U}_h + \mathbf{M}\widetilde{\boldsymbol{f}}_h\left(\boldsymbol{U}_h\right) = \mathbf{0},$$

where $\widetilde{\boldsymbol{f}}_h\left(\boldsymbol{U}_h\right)$ is the vector with entries given by $\left(\widetilde{\boldsymbol{f}}_h\left(\boldsymbol{U}_h\right)\right)_i := \mathrm{dof}_i\left(\widetilde{f}_h(u_h)\right)$. Note that, as in the ideal case, the entries of $\widetilde{\boldsymbol{f}}_h\left(\boldsymbol{U}_h\right)$ associated with the boundary DoFs can be computed evaluating $f(\cdot)$ at the corresponding entries of the vector $\boldsymbol{U}_h$. As a result, the nonlinear substeps in the fully-discrete SS-OS scheme (4.3a, 4.3b, 4.3c) can be solved in a static condensation fashion in two consecutive steps:

1. We first solve the independent one dimensional nonlinear equations associated with the boundary DoFs as in (4.4a, 4.4b).
2. Using the computed values of the boundary DoFs, we solve a set of independent small nonlinear systems involving just the internal-moment DoFs on those elements $E \in \mathcal{T}_h$ where the condition $k < \eta_E$ is not satisfied. More specifically, for each element E such that $k \geq \eta_E$, let $\boldsymbol{U}_{h,E}$ be the vector coefficient of the representation of $u_h|_E$. As the components of $\boldsymbol{U}_{h,E}$ associated with the boundary DoFs are already available from the previous step, it only remains to find the components associated with internal-moment DoFs that satisfy

$$\boldsymbol{U}^{(2)}_{h,E} = \boldsymbol{U}^{(1)}_{h,E} - \frac{\tau}{2}\left(\widetilde{\boldsymbol{f}}_h\left(\boldsymbol{U}^{(1)}_{h,E}\right) + \widetilde{\boldsymbol{f}}_h\left(\boldsymbol{U}^{(2)}_{h,E}\right)\right). \tag{5.2}$$

We recall that by definition (5.1b), the evaluation of $\widetilde{\boldsymbol{f}}_h\left(\boldsymbol{U}_{h,E}\right)$ requires the computation of $\pi^0_{k,E}\left(u_h\right)$ which is a local projection, i.e., it is computable using only the components of $\boldsymbol{U}^{(2)}_{h,E}$. Therefore, it is clear that the system (5.2) is completely local and as such it can be solved separately for each element $E \in \mathcal{T}_h$ such that $k \geq \eta_E$.

Evidently, the above procedure is still highly parallelizable.

Remark 4 The actual computation of η_E for each $E \in \mathcal{T}_h$ is an important and delicate issue in the implementation of the S-VEM. In practice, it is also necessary to be careful with small or almost aligned edges for stability reasons. We briefly recall the most used strategies in the S-VEM literature [10, 11]. The *lazy* choice consists in using always internal moments of degree up to $k-3$, as by definition $\eta_E \geq 3$. A second strategy called the *stingy* choice consists in fixing a minimum angle $\theta_0 > 0$ and then, considering as "different" straight lines those associated with consecutive edges whose internal angle is smaller than θ_0. One last strategy, is the *adaptive stingy* choice, that in addition to the angle treshold θ_0, also impose an edge ratio ρ_0 and neglects those edges e of E satisfying $|e| < \rho_0 h_E$. Needlessly to say, a *stingy* or *adaptive stingy* choice would be more appropriate for the proposed method, as the additional cost of computing the "exact" value of η_E is evidently negligible compared to the cost of evaluating the nonlinear term on each time step using numerical quadratures.

6 Numerical experiments

In this section we present some numerical experiments to show the accuracy and efficiency of the proposed scheme. An object oriented implementation in MATLAB was developed for high order approximations on general polygonal meshes. As time marching scheme we use the SS-OS method (4.2a, 4.2b) presented in Sect. 4. All the linear systems were solved with the preconditioned conjugate gradient (PCG) method. The incomplete Cholesky factorization with a drop tolerance of 10^{-5} was used as preconditioner. Linear and nonlinear systems were solved with a tolerance of 10^{-10} as stopping criteria; and numerical quadratures for each polygon were

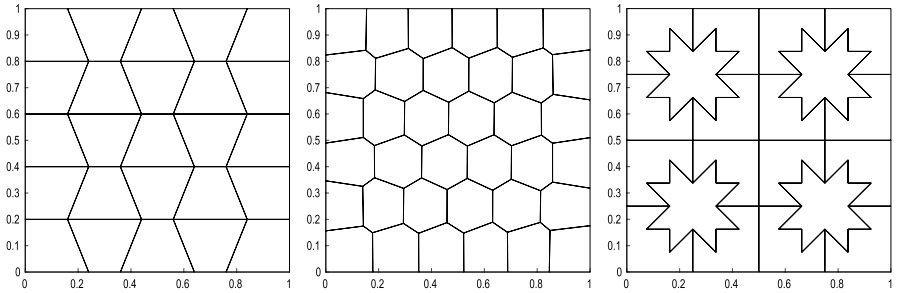

(a) Distorted squares mesh. **(b)** Voronoi mesh. **(c)** Non-convex mesh.

Fig. 2 Example of meshes used in the numerical experiments

obtained using the Vianello approach [31]. The sets of meshes used in all the experiments are exemplified in Fig. 2. Note that, for these meshes, the values of η_E can be known *a-priori*, as for strictly convex N-sided polygons $\eta_E = N$ and all the non-convex polygons in Fig. 2a satisfy $\eta_E \geq 8$.

In order to illustrate the accuracy and efficiency of the proposed method, we will compare our results with those obtained for the enhanced VEM proposed in [1]. While the linear substeps of the SS-OS time marching scheme are similar for both versions, the nonlinear substeps for the method in [1] require to solve the following strongly coupled system of nonlinear equations

$$\mathbf{M}\boldsymbol{U}_h^{(2)} = \mathbf{M}\boldsymbol{U}_h^{(1)} - \frac{\tau}{2}\left(\boldsymbol{F}_h\left(\boldsymbol{U}_h^{(1)}\right) + \boldsymbol{F}_h\left(\boldsymbol{U}_h^{(2)}\right)\right), \tag{6.1}$$

where $\boldsymbol{F}_h(\cdot)$ is the nonlinear operator defined as

$$\left(\boldsymbol{F}_h(\boldsymbol{U}_h), V_h\right)_{l_2} := m\left(\pi_k^0\left(f(\pi_k^0(u_h))\right); v_h\right) \quad \forall v_h \in V_k^S(\mathcal{T}_h).$$

The nonlinear systems (6.1) will be solved using a semilinear iterative method, that avoids computing the Jacobian of the nonlinear term. Each linear iteration s consists in solving the following linear system

$$\mathbf{M}\boldsymbol{U}_h^{(2,s+1)} = \mathbf{M}\boldsymbol{U}_h^{(1)} - \frac{\tau}{2}\left(\boldsymbol{F}_h\left(\boldsymbol{U}_h^{(1)}\right) + \boldsymbol{F}_h\left(\boldsymbol{U}_h^{(2,s)}\right)\right).$$

On the other hand, the reported execution times correspond to computations carried out on a DELL laptop with an Intel Core i7-8750h processor, 32Gb of RAM and Linux operating system.

6.1 Accuracy test

As first experiment we numerically asses the accuracy of the proposed method. We consider a manufactured problem on $Q_T = (0,1)^2 \times (0,1]$ with a

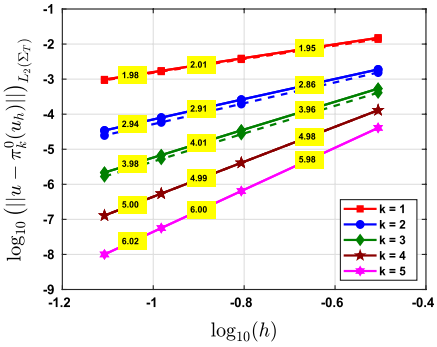

(a) Distorted squares meshes.

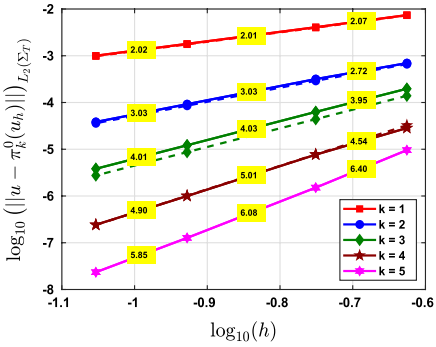

(b) Voronoi meshes.

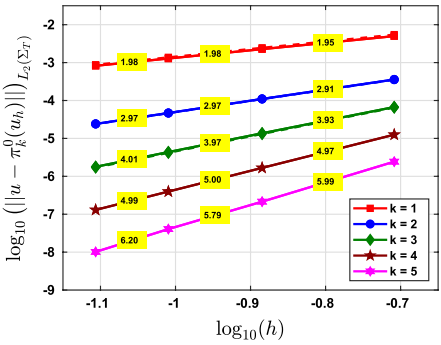

(c) Non-convex meshes.

Fig. 3 Rates of convergence at $T = 1$ for the test problem 6.1 obtained for the proposed method (continuous line) and the enhanced VEM in [1] (dashed line). The numbers in the yellow rectangles are the algebraic convergence rates in h and non-visible lines were overlapped

nonlinear term $f(u) = 1/(1+u^2)$, adding a source term so the exact solution be $u(x, y, t) = e^{-t}\cos(\pi x)\cos(\pi y)$.

In Fig. 3 we present the errors in the L_2-norm with respect to $\pi_k^0(u_h)$ at the final time T, i.e., at $\Sigma_T := \Omega \times \{T\}$, for each kind of mesh. In the same plot we have included the errors obtained by the enhanced VEM in [1] as reference; and no significant difference in terms of accuracy is observed. Optimal rates of convergence of order $\mathcal{O}\left(h^{k+1}\right)$ are obtained as stated in Theorem 1. The time step was taken as $\tau = \mathcal{O}\left(h^{(k+1)/2}\right)$ in order to equilibrate the errors in space and time.

To evaluate the temporal accuracy of the fully-discrete scheme, we use a sequence of time refinements with $\tau = 1.25 \times 10^{-1}$, 6.25×10^{-2}, 3.125×10^{-2}, 1.5625×10^{-2}; and in order to let the time error dominate, computations were carried out for the finest voronoi mesh and $k = 4$. The obtained rates of convergence for the $\mathcal{DRD}$ and the $\mathcal{RDR}$ splitting methods are shown in Fig. 4 and validate the second order in time $\mathcal{O}\left(\tau^2\right)$ accuracy of the SS-OS fully-discrete scheme. In this experiment, better

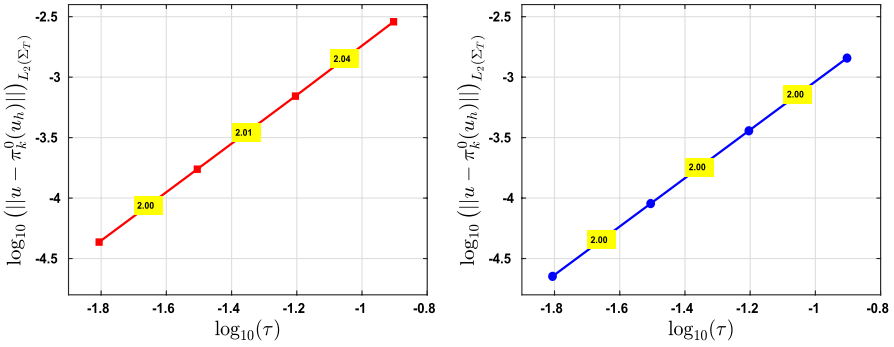

(a) $\mathcal{DRD}$. **(b)** $\mathcal{RDR}$.

Fig. 4 Time accuracy of the proposed method at $T = 1$ for the test problem 6.1 of both versions of the fully-discrete scheme (4.2a, 4.2b)

Table 1 Comparison in terms of the number of degrees of freedom of the S-VEM and the enhanced VEM in [1] for the test problem 6.1

Mesh type	Distorted squares		Voronoi		Non-convex	
	S-VEM	VEM [1]	S-VEM	VEM [1]	S-VEM	VEM [1]
			$k=2$			
m_1	**96**	121	**183**	219	**189**	209
m_2	**341**	441	**323**	387	**721**	801
m_3	**736**	961	**723**	867	**1597**	1777
m_4	**1281**	1681	**1283**	1539	**2817**	3137
			$k=3$			
m_1	**156**	231	**292**	400	**293**	353
m_2	**561**	861	**516**	708	**1121**	1361
m_3	**1216**	1891	**1156**	1588	**2485**	3025
m_4	**2121**	3321	**2052**	2820	**4385**	5345
			$k=4$			
m_1	⋆ **241**	366	⋆ **407**	617	**397**	517
m_2	⋆ **881**	1381	⋆ **717**	1093	**1521**	2001
m_3	⋆ **1921**	3046	⋆ **1601**	2453	**3373**	4453
m_4	⋆ **3361**	5361	⋆ **2837**	4357	**5953**	7873
			$k=5$			
m_1	⋆ **351**	526	⋆ **538**	870	**501**	701
m_2	⋆ **1301**	2001	⋆ **940**	1542	**1921**	2721
m_3	⋆ **2851**	4426	⋆ **2080**	3462	**4261**	6061
m_4	⋆ **5001**	7801	⋆ **3668**	6150	**7521**	10721

The red star symbol ⋆ indicates that the extended version from Sect. 5 is needed

Bold is used to highlight the small number of DoFs for the S-VEM compared to the original VEM

accuracy is observed for the $\mathcal{RDR}$ splitting. Not shown here, similar results were obtained for the other meshes.

In Table 1, we compare the number of global degrees of freedom for the S-VEM and the enhanced VEM in [1], where naturally the reduction in the number of degrees of freedom depends on the mesh and a more noticeable reduction is obtained at increasing k. This is also illustrated in Fig. 5, where we compare the accuracy of both methods with respect to the number of DoFs.

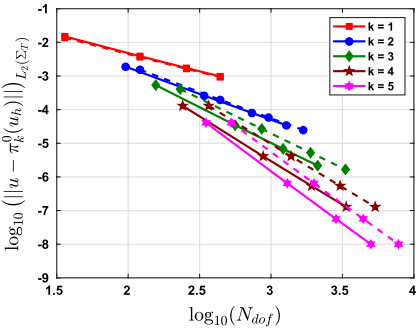

(a) Distorted squares meshes.

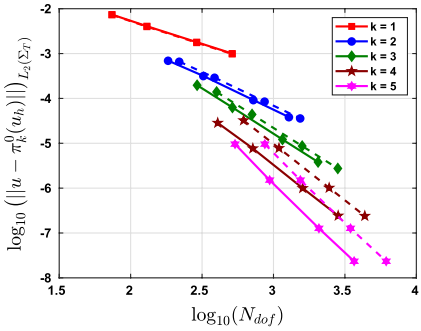

(b) Voronoi meshes.

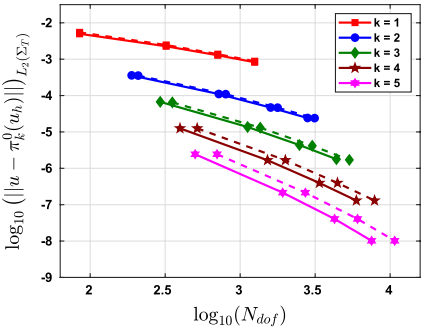

(c) Non-convex meshes.

Fig. 5 Rates of convergence at $T = 1$ for the test problem 6.1 obtained by the proposed method (continuous line) and the enhanced VEM in [1] (dashed line) in terms of the number of DoFs

6.2 Efficiency test

In this experiment we consider the following Allen-Cahn equation on $Q_T = (0,1)^2 \times (0, 22.5]$ as in [1]:

$$\frac{\partial u}{\partial t} - \epsilon \Delta u + u^3 - u = 0, \qquad \text{in } Q_T, \tag{6.2a}$$

$$\nabla u \cdot \boldsymbol{n} = 0, \qquad \text{on } \partial\Omega \times (0,T), \tag{6.2b}$$

$$u(x,y,0) = \cos(2\pi x^2)\cos(2\pi y^2), \text{ in } \Omega, \tag{6.2c}$$

where the nonlinear term $f(u) = u^3 - u$ only satisfies a local Lipschitz condition. In fact, the error estimate in Theorem 1 is still valid if $f(\cdot)$ is only locally Lipschitz continuous under the additional assumption of both the exact and the approximated solutions to be bounded.

In order to show the efficiency of the proposed method, we compare our results with those obtained for the interpolatory VEM in [3] and the enhanced VEM in [1]. In all these experiments, we consider the finest meshes of each kind, $\tau = 5 \times 10^{-3}$ as time step and the $\mathcal{RDR}$ splitting.

Table 2 CPU execution times for the Allen-Cahn equation (6.2a, 6.2b, 6.2c) in the test problem 6.2 with $\epsilon = 0.01$, for the proposed S-VEM and the interpolatory VEM in [3] with $k = 1$

Linear substeps			Nonlinear substeps			Total		
S-VEM (sec)	VEM[3] (sec)	Ratio	S-VEM (sec)	VEM [3] (sec)	Ratio	S-VEM (sec)	VEM[3] (sec)	Ratio
Distorted squares mesh								
2.8	2.6	**0.9**	1.6	39.7	**24.8**	4.4	42.3	**9.6**
Voronoi mesh								
3.1	2.9	**0.9**	1.5	48.8	**32.5**	4.6	51.7	**11.2**
Non-convex mesh								
6.6	6.6	**1.0**	2.3	163.5	**71.1**	8.9	107.1	**12.0**

Bold is used to highlight the ratios that indicate how faster the proposed method performs compared to other VEM discretizations

In Table 2 we report the CPU execution times for the approximation of the Allen-Cahn equation (6.2a, 6.2b, 6.2c) with $\epsilon = 0.01$ for the proposed method and the interpolatory VEM presented in [3]. We recall that the method in [3] is limited to $k = 1$ and does not include the stability part of the nonlinear term, so the nonlinear systems in the SS-OS fully-discrete scheme (4.2a, 4.2b) remain coupled. We observe that the times in the linear substeps are approximately equal in both cases, which is expected as both methods have the same number of DoFs. However, for the nonlinear substeps our method performs about 20 to 70 times faster depending on the mesh; and a total boost of approximately 10 times is obtained in all the cases.

In a similar way, in Table 3 we compare the CPU execution times for the proposed method and the enhanced VEM in [1] with different degrees of approximation.

Table 3 CPU execution times for the Allen-Cahn equation (6.2a, 6.2b, 6.2c) in the test problem 6.2 with $\epsilon = 0.01$, for the proposed S-VEM and the enhanced VEM in [1]

	Linear substeps			Nonlinear substeps			Total		
k	S-VEM (sec)	VEM [1] (sec)	Ratio	S-VEM (sec)	VEM [1] (sec)	Ratio	S-VEM (sec)	VEM [1] (sec)	Ratio
Distorted squares mesh									
2	16.5	22.1	**1.3**	3.6	374.8	**104.1**	20.1	396.9	**19.8**
3	41.5	107.4	**2.6**	5.3	1243.4	**234.6**	46.8	1350.8	**28.9**
⋆ 4	48.9	941.0	**19.2**	208.5	9483.4	**45.5**	257.4	10424.4	**40.5**
Voronoi mesh									
2	9.6	13.4	**1.4**	2.2	210.5	**95.7**	11.8	223.9	**19.0**
3	30.4	66.0	**2.2**	3.2	758.3	**237.0**	33.6	824.3	**24.5**
⋆ 4	139.3	570.0	**4.1**	20.1	3366.7	**167.5**	159.4	3936.7	**24.7**
Non-convex mesh									
2	54.6	66.6	**1.2**	6.3	687.5	**109.1**	60.9	754.1	**12.4**
3	111.8	642.3	**5.8**	7.5	5426.4	**723.5**	119.3	6068.7	**50.9**
4	197.2	2404.4	**12.2**	8.3	21388.8	**2577.0**	205.5	23793.2	**115.8**

The red star symbol ⋆ indicates that the extended version from Sect. 5 is needed

Bold is used to highlight the ratios that indicate how faster the proposed method performs compared to other VEM discretizations

Since the proposed method requires less DoFs, it performs faster for the linear substeps. As for the nonlinear substeps, our method performs from 40 to 2500 times faster depending on the mesh and the degree of accuracy. A total boost of about 12 to 110 times is obtained. For each mesh, we have indicated those degrees where some internal moment DoFs are needed; in such cases, the extended version from Sect. 5 was used and a significant improvement in the efficiency of the method is still observed. The substantial reduction obtained for the non-convex mesh is a consequence of the high number of quadrature points required for the VEM in [1] to compute the nonlinear term on each time step.

In Fig. 6 we show the evolution of the approximated solution $\pi_k^0(u_h)$ for the Allen-Cahn equation with $\epsilon = 0.01$, which is expected to converge to its stable state $u = -1$. The plots portray the same behaviour observed in [1] for the enhanced VEM.

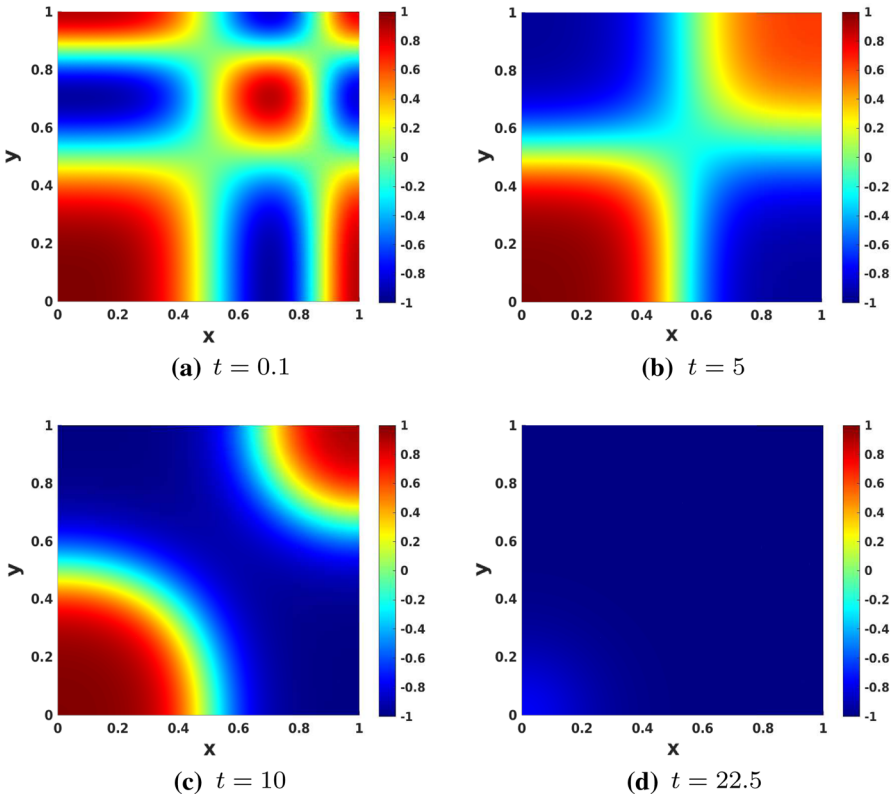

(a) $t = 0.1$ **(b)** $t = 5$

(c) $t = 10$ **(d)** $t = 22.5$

Fig. 6 Snapshots of the approximation $\pi_k^0(u_h)$ for the Allen-Cahn equation (6.2a, 6.2b, 6.2c) with $\epsilon = 0.01$, in the test problem 6.2

7 Conclusions

In this work, an interpolatory Serendipity Virtual Element method for semilinear parabolic problems on polygonal meshes is proposed. A significant reduction in the computational cost of the method is obtained by approximating the nonlinear term with an element in the S-VEM space. Optimal error estimates of order $\mathcal{O}\left(h^{k+1}\right)$ in the L_2-norm are proven for the semi-discrete formulation.

To exploit the structure of the system of nonlinear differential equations arising from the semi-discrete formulation, we use a second order operator splitting time marching scheme, which decouples the linear and nonlinear terms. In the ideal case, with only boundary DoFs, the nonlinear substeps consist in solving a set of completely independent one dimensional nonlinear equations; while in the extension proposed to the case when some internal-moment DoFs are required, it is also necessary to solve an additional set of independent small nonlinear systems on each element of the mesh that does not satisfy the condition of the ideal case. Our numerical experiments validate the optimal convergence of the method and the improvement in efficiency respect to the enhanced VEM in [1].

The extension to three dimensional problems using the S-VEM spaces presented in [10]; as well as the analysis and a proper comparison of different time discretizations is an ongoing work.

Funding Open access funding provided by Università degli Studi di Pavia within the CRUI-CARE Agreement.

Declarations

Conflict of interest This research did not receive any specific grant from funding agencies in the public, commercial, or not-for-profit sectors. The authors have no competing interests to declare that are relevant to the content of this article.

References

1. Adak, D., Natarajan, E., Kumar, S.: Convergence analysis of virtual element methods for semilinear parabolic problems on polygonal meshes. Num. Meth. PDEs **35**(1), 222–245 (2019)
2. Adak, D., Natarajan, E., Kumar, S.: Virtual element method for semilinear hyperbolic problems on polygonal meshes. Int. J. Comp. Math. **96**(5), 971–991 (2019)

3. Adak, D., Natarajan, S.: Virtual element method for semilinear sine-Gordon equation over polygonal mesh using product approximation technique. Math. Comp. Simul. **172**, 224–243 (2020)
4. Adak, D., Natarajan, S.: Virtual element methods for nonlocal parabolic problems on general type of meshes. Adv. Comp. Math. **46**(5), 46–74 (2020)
5. Adak, D., Natarajan, S., Natarajan, E.: Virtual element method for semilinear elliptic problems on polygonal meshes. Appl. Num. Math. **145**, 175–187 (2019)
6. Ahmad, B., Alsaedi, A., Brezzi, F., Marini, D., Russo, A.: Equivalent projectors for virtual element methods. Comp. Math. Appl. **66**(3), 376–391 (2013)
7. Anaya, V., Bendahmane, M., Mora, D., Sepúlveda, M.: A virtual element method for a nonlocal Fitzhugh-Nagumo model of cardiac electrophysiology. IMA J. Num. Anal. **40**(2), 1544–1576 (2020)
8. Antonietti, P., Beirão da Veiga, L., Scacchi, S., Verani, M.: A c1 virtual element method for the Cahn-Hilliard equation with polygonal meshes. SIAM J. Num. Anal. **54**(1), 34–56 (2016)
9. Beirão da Veiga, L., Brezzi, F., Cangiani, A., Manzini, G., Marini, L., Russo, A.: Basic principles of virtual element methods. Math. Models Methods Appl. Sci. **23**(01), 199–214 (2013)
10. Beirão da Veiga, L., Brezzi, F., Dassi, F., Marini, L., Russo, A.: Serendipity virtual elements for general elliptic equations in three dimensions. Chin. Ann. Math. Ser. B **39**(2), 315–334 (2018)
11. Beirão da Veiga, L., Brezzi, F., Marini, L., Russo, A.: Serendipity nodal VEM spaces. Comput. Fluids **141**, 2–12 (2016)
12. Beirão da Veiga, L., Lovadina, C., Russo, A.: Stability analysis for the virtual element method. Math. Models Methods Appl. Sci. **27**(13), 2557–2594 (2017)
13. Brenner, S., Scott, L.: The mathematical theory of finite element methods, vol. 3. Springer, Berlin (2008)
14. Cangiani, A., Chatzipantelidis, P., Diwan, G., Georgoulis, E.: Virtual element method for quasilinear elliptic problems. IMA J. Num. Anal. **40**(4), 2450–2472 (2020)
15. Castillo, P., Gómez, S.: Interpolatory super-convergent discontinuous Galerkin methods for nonlinear reaction diffusion equations on three dimensional domains. Commun. Nonl. Sci. Num. Simul. **90**(C), 105388 (2020)
16. Castillo, P., Gómez, S.: An interpolatory directional splitting-local discontinuous Galerkin method with application to pattern formation in 2D/3D. Appl. Math. Comp **397**(C), 125984 (2021)
17. Chen, L., Huang, J.: Some error analysis on virtual element methods. Calcolo **55**(1), 1–23 (2018)
18. De Bellis, M., Wriggers, P., Hudobivnik, B.: Serendipity virtual element formulation for nonlinear elasticity. Comp. Struct. **223**, 106094 (2019)
19. Dehghan, M., Gharibi, Z.: Virtual element method for solving an inhomogeneous Brusselator model with and without cross-diffusion in pattern formation. J. Sci. Comput. **89**(1), 1–31 (2021)
20. Douglas, J., Dupont, T.: The effect of interpolating the coefficients in nonlinear parabolic Galerkin procedures. Math. Comp. **29**(130), 360–389 (1975)
21. Frittelli, M., Madzvamuse, A., Sgura, I.: Bulk-surface virtual element method for systems of PDEs in two-space dimensions. Numer. Math. **147**(2), 305–348 (2021)
22. Gatica, G., Munar, M., Sequeira, F.: A mixed virtual element method for a nonlinear Brinkman model of porous media flow. Calcolo **55**(2), 1–36 (2018)
23. Kobayashi, R.: Modeling and numerical simulations of dendritic crystal growth. Phys. D: Nonlinear Phenomena **63**(3–4), 410–423 (1993)
24. Liu, X., He, Z., Chen, Z.: A fully discrete virtual element scheme for the Cahn-Hilliard equation in mixed form. Comp. Phys. Commun. **246**, 106870 (2020)
25. Marcon, L., Sharpe, J.: Turing patterns in development: what about the horse part? Curr. Opin. Genetics Dev. **22**(6), 578–584 (2012)
26. Mascotto, L.: Ill-conditioning in the virtual element method: stabilizations and bases. Num. Meth. Part. Diff. Eqs. **34**(4), 1258–1281 (2018)
27. Mikhailov, A., Showalter, K.: Control of waves, patterns and turbulence in chemical systems. Phys. Reports **425**(2–3), 79–194 (2006)
28. Munar, M., Sequeira, F.: A posteriori error analysis of a mixed virtual element method for a nonlinear Brinkman model of porous media flow. Comp. Math. Appl. **80**(5), 1240–1259 (2020)
29. Neubert, M., Caswell, H.: Demography and dispersal: calculation and sensitivity analysis of invasion speed for structured populations. Ecology **81**(6), 1613–1628 (2000)
30. Russo, A.: On the choice of the internal degrees of freedom for the nodal virtual element method in two dimensions. Comp. Math. Appl. **72**(8), 1968–1976 (2016)
31. Sommariva, A., Vianello, M.: Product Gauss cubature over polygons based on Green's integration formula. BIT Num. Math. **47**(2), 441–453 (2007)

32. Strang, G.: On the construction and comparison of difference schemes. SIAM J. Num. Anal. **5**(3), 506–517 (1968)
33. Tenno, A., Tenno, R., Suntio, T.: Charge-discharge behaviour of VRLA batteries: model calibration and application for state estimation and failure detection. J. Power Sources **103**(1), 42–53 (2001)
34. Turing, A.: The chemical basis of morphogenesis. Bull. Math. Biol. **52**(1), 153–197 (1990)
35. Vacca, G., Beirão da Veiga, L.: Virtual element methods for parabolic problems on polygonal meshes. Num. Meth. Part. Diff. Eqs. **31**(6), 2110–2134 (2015)